



Contents lists available at ScienceDirect

Journal of Quantitative Spectroscopy & Radiative Transfer

journal homepage: www.elsevier.com/locate/jqsrt

An efficient method for computing atmospheric radiances in clear-sky and cloudy conditions

Xiuhong Chen^a, Heli Wei^{a,*}, Ping Yang^b, Zhonghai Jin^c, Bryan A. Baum^d

^a Key Laboratory of Atmospheric Composition and Optical Radiation, Anhui Institute of Optics and Fine Mechanics, the Chinese Academy of Sciences, P.O. Box 1125, Hefei, Anhui 230031, China

^b Department of Atmospheric Sciences, Texas A&M University, College Station, TX 77843, USA

^c AS&M, Incorporated, Hampton, VA 23666, USA

^d Space Science and Engineering Center, University of Wisconsin Madison, Madison, WI 53706, USA

ARTICLE INFO

Article history:

Received 4 June 2010

Received in revised form

19 August 2010

Accepted 20 August 2010

Keywords:

Computationally efficient method

Spectral radiances

Multiple scattering

ABSTRACT

A computationally efficient method is developed to simulate the radiances in a scattering and absorbing atmosphere along an arbitrary path in the spectral region ranging from visible to far-infrared with a spectral resolution of 1 cm^{-1} . For a given spectral region, the method is based on fitting radiances pre-calculated from the discrete ordinate radiative transfer (DISORT) at several wavenumbers. Radiances at other wavenumbers are interpolated based on the pre-computed total absorption and scattering optical thicknesses and the surface albedo. The computational efficiency and accuracy of the method are tested in comparison with rigorous simulations for various scenarios under the same conditions. For both clear-sky and cloud atmospheres, the present method is at least 140 times faster than the direct application of DISORT. Across the spectral range, the standard relative differences between the new method and the DISORT are less than 2% for clear-sky conditions. Root-mean-square (RMS) differences of the top of the atmosphere (TOA) brightness temperatures between the new method and DISORT, for atmospheric infrared sounder (AIRS) channels over clear-sky, ice cloudy and water cloudy skies, are within the noise equivalent differential temperature (NEDT) of the AIRS sensor. The fast method is also applied to simulations of the spectral downwelling radiance measured by the Fourier transform infrared (FTIR) interferometer, and to the simulations of the AIRS upwelling radiances under clear-sky and cloudy conditions.

© 2010 Elsevier Ltd. All rights reserved.

1. Introduction

The discrete ordinate radiative transfer (DISORT) [1] is a rigorous method for simulating the transfer of radiation in a vertically inhomogeneous, non-isothermal, plane-parallel medium. However, it is not computationally efficient to use DISORT for many applications, especially those involving analysis of hyper-spectral infrared (IR)

data from satellite sensors such as the atmospheric infrared sounder (AIRS) and the infrared atmospheric sounding interferometer (IASI). Computational efficiency is as important as accuracy for the radiative transfer calculations in many practical applications including numerical weather prediction, climate sensitivity studies and remote sensing. For example, in the retrieval of temperature and humidity profiles from AIRS or IASI measurements, the data at a large number of channels must be processed via an efficient means.

Numerous approximate methods have been developed to enhance the computational efficiency of radiative

* Corresponding author. Tel.: +86 551 559 1535;

fax: +86 551 559 1572.

E-mail address: hlwei@aiofm.ac.cn (H. Wei).

transfer models. For example, the two-stream and four-stream approximations have been widely used by the radiative transfer community [2,3]. However, the relative errors of the two-stream approximation can be as large as 15–20%, as illustrated by King and Harshvarhan [4]. The four-stream approximation does enhance the accuracy in comparison with the two-stream approximation, but is less computationally efficient [5]. Furthermore, the two-stream and four-stream approximations are usually applied to the simulation of atmospheric radiative fluxes rather than to radiances. Other fast methods, such as those developed by Wei et al. [6], Niu et al. [7] and Zhang et al. [8], use pre-computed look-up tables (LUTs) of the reflection function, transmission function, and emissivity to alleviate the computational burden. These approaches are more efficient and accurate than a simple approximation to account for the effect of multiple scattering. However, the focus of these methods is primarily on the IR spectrum with application to the simulation of the top of the atmosphere (TOA) and/or surface radiances. Moncet and Clough [9,10] developed an accelerated monochromatic radiative transfer model for application to scattering atmospheres, using the adding-doubling method in both solar and thermal regimes. Their method has been applied to high spectral resolution simulations by constructing tables of the adding-doubling solution versus absorption over certain finite spectral intervals.

This paper reports on a computationally efficient method (hereafter, referred to as the efficient method for atmosphere scattering radiance, or, EMASR) for spectral radiance calculations along an arbitrary path in a scattering atmosphere. In this method, the atmospheric transmittance and thermal radiances are obtained from a clear-sky atmosphere radiative transfer model (CSRTM) [11], with a spectral resolution of 1 cm^{-1} and in the spectral region from 1 to $25,000\text{ cm}^{-1}$ divided into 13 sub-regions. In each sub-region, the total absorption optical thickness τ_a and the total scattering optical thickness τ_s along a path are computed from the CSRTM. τ_a values are sorted in ascending order. The layer absorption optical thickness $\tau_{a,l}$ (subscript l indicates the number of a specific atmospheric layer) and the layer scattering optical thickness $\tau_{s,l}$ from the top of the atmosphere to a user-defined height are input into DISORT to obtain the radiances in a scattering atmosphere. In numerical computations, the total column absorption optical thickness τ_a is logarithmically spaced. Radiances at other wavenumbers are interpolated in the domain of the column absorption optical thickness τ_a , column scattering optical thickness τ_s , and the surface albedo. The computational efficiency and accuracy of this method are tested in comparison with the direct use of DISORT in conjunction with CSRTM.

In Section 2, we present a detailed method to compute the scattered radiance, including expressing scattered radiance in terms of a smoothly varying function of other parameters, dividing sub-spectra, and fitting radiation spectra. The accuracy and computer CPU time requirements for this method are presented in Section 3. In Section 4, we show the comparisons of the EMASR with observed downwelling IR spectral radiance and brightness

by Fourier transform infrared (FTIR) interferometer. We apply the present fast method to a cloudy atmosphere with a layer of ice clouds or water clouds, and we simulate the atmospheric infrared sounder (AIRS) cloudy radiances in Section 5. This study is summarized and briefly discussed in Section 6.

2. Methodology

The total atmospheric radiances include contributions from a thermal radiance component (consisting of thermal path radiance, surface emission, and thermal scattered radiance), from scattered solar radiation, and from surface reflection. The various components may coexist in the same waveband or have greater or lesser importance in different wavebands. The thermal radiance occurs mainly at infrared wavelengths (from 1 to 5000 cm^{-1}) in the spectral range from 0.4 to $10,000\text{ }\mu\text{m}$ (or, from 1 to $25,000\text{ cm}^{-1}$ in the wavenumber domain), whereas radiance scattered by molecules and aerosols occurs at visible and near-infrared wavelengths (from 2001 to $25,000\text{ cm}^{-1}$). The scattering of radiation by clouds occurs over the entire spectral domain. In this study, the scattering and absorption of radiation by atmospheric molecules and aerosols, as well as clouds are included in the CSRTM.

The radiance associated with the scattering of molecules and aerosols and the reflection by the surface with 1 cm^{-1} spectral resolution is computed from DISORT in conjunction with CSRTM. Consequently, a fitting method is used, aimed at enhancing computational efficiency.

For a clear-sky atmosphere, the optical thickness τ_s associated with molecular or aerosol scattering varies smoothly with wavenumber within a sub-region, whereas the absorption optical thickness τ_a associated with molecular absorption can vary much more abruptly with wavenumber even in a narrow subspectrum. Within a sub-region, the radiance contribution of the multiple scattering may vary smoothly with τ_s , τ_a , or the total optical thickness ($\tau = \tau_s + \tau_a$). Thus, it is not necessary to account for multiple scattering at all wavenumbers. If we compute the radiances at several wavenumbers, radiances at other wavenumbers can be interpolated according to the pre-computed τ_a and τ_s for a given path. To conduct the interpolation, the key to the present method is to find a smoothly varying function that represents the scattering radiances within a sub-region.

To define the smoothly varying function, we calculate a waveband of spectral radiances using DISORT. In DISORT computations, the entire atmosphere from the surface to a height of 120 km is divided into 50 vertically inhomogeneous layers. The physical thickness of each layer varies from 1 to 5 km, and the surface is assumed to be Lambertian. The surface albedo varies with wavenumber for various surface types, such as snow, ocean, grass, forest, and desert. The optical thicknesses with 1 cm^{-1} spectral resolution for each layer are calculated using the CSRTM. The calculated optical thicknesses include the scattering, absorbing, and continuum absorbing of molecules (τ_{ms} , τ_{ma} , τ_{mc}), and the scattering and absorption of

aerosols (τ_{as} , τ_{aa}). The single-scattering albedo $\omega(i)$ of the i th layer of the atmosphere can be expressed as

$$\omega(i) = \frac{\tau_s(i)}{\tau_s(i) + \tau_a(i)} = \frac{\tau_{ms}(i) + \tau_{as}(i)}{\tau_{ms}(i) + \tau_{ma}(i) + \tau_{mc}(i) + \tau_{as}(i) + \tau_{aa}(i)}. \quad (1)$$

The scattering phase function for the i th layer of molecules is

$$p_m(i) = \frac{3}{4}(1 + \cos^2 \Theta), \quad (2)$$

where Θ is the scattering angle. The scattering phase function $p_a(i)$ for the i th layer of aerosols can be computed using the Lorentz–Mie code for a specific size distribution, or using the Henyey–Greenstein (H–G) phase function given by

$$p_a(i) = \frac{1 - g^2}{(1 + g^2 - 2g \cdot \cos \Theta)^{3/2}}, \quad (3)$$

where g is the asymmetry factor. The averaged scattering phase function for the i th layer can be weighted according to the combinations of $\tau_{ms}(i)$ of molecules and $\tau_{as}(i)$ of aerosols as follows:

$$p(i) = \frac{\tau_{ms}(i) \cdot p_m(i) + \tau_{as}(i) \cdot p_a(i)}{\tau_{ms}(i) + \tau_{as}(i)} \quad (4)$$

The averaged phase function can be expanded in terms of a series of the Legendre polynomials by using the δ -fit method developed by Hu et al. [12]. In this study, 16 streams are used in the scattering phase function expansion and also in the simulation of atmospheric radiances.

Upward radiance R at the top of the atmosphere (TOA) and the total optical thickness τ as a function of wavenumber in the sub-region from 9001 to 13,000 cm^{-1} are shown in Fig. 1. In this sub-region, R varies strongly with wavenumber owing to the combined effect of atmospheric absorption and scattering. The figure also shows that τ varies with wavenumber in a reverse form with R .

To analyze the variation between R and τ , τ are sorted with R in an ascending order, shown in Fig. 2(a). We find that the R depends on τ , but varies abruptly from τ for

some cases. Thus, R cannot be singularly determined by τ . To find a singular dependence relationship of R on combined parameters, we have examined several parameters and their combinations, such as τ_s , τ_a , and surface albedo. For the case of upward radiance from the surface, the radiance reflected by the surface must be included, while for the case of downward radiance at the surface or an arbitrary path between two points above the surface, τ_s and τ_a play more important roles. The two scenarios are treated separately. For the case of upward radiances reflected from the surface, the radiances R are divided by surface albedo, referred to as R' , while for other cases, the radiances R are divided by τ_s and τ_a , referred to as R'' . After these treatments, R' or R'' is sorted in ascending order with τ_a similar to Fig. 2(a). We analyze the relationship between R' or R'' and τ_a , with the results of R' vs. τ_a shown in Fig. 2(b) and the results of R'' vs. τ_a shown in Fig. 2(c) for each of the sub-regions. Both R' and R'' are smooth functions of τ_a (with cases 1–11 referring to each of the sub-regions between 1 and 25,000 cm^{-1}). From Fig. 2, it can be seen that R' or R'' can be represented as a smoothly varying function of the atmospheric absorption optical thickness. The functional relationship of R' or R'' to τ_a can be used to quickly compute the scattering radiances with each sub-spectrum. Thus, we can use values for several wavenumber nodes (supplied by DISORT) to obtain values at the other nodes by using a fitting method. The actual radiance R is obtained by multiplying the values of R' or R'' with either the albedo or with the τ_s and τ_a .

The full spectral region is divided into sub-regions, and the optimal width of each sub-region needs to be determined. The accuracy and computational efficiency of the proposed EMASR are related to the width of the sub-regions. We find more sub-regions (narrower band interval) enhance the accuracy but reduce the efficiency, therefore, the accuracy appears to compete with the computational efficiency. At wavenumbers larger than 5000 cm^{-1} , τ_s and surface albedo are smoother than those for wavenumbers smaller than 5000 cm^{-1} , thus, sub-regions with wavenumbers less than or greater than

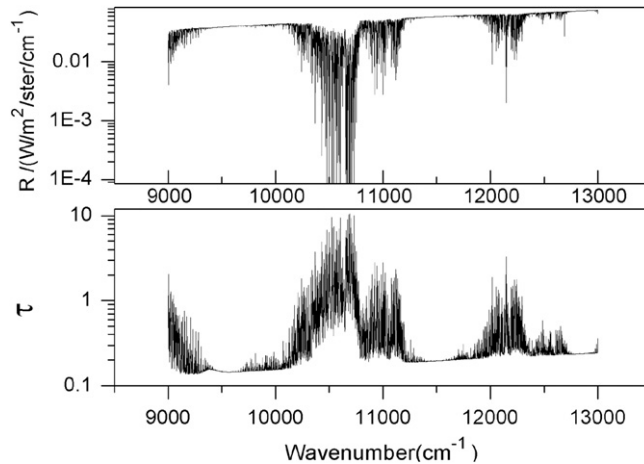


Fig. 1. The radiance and the total optical thickness as a function of wavenumber (downward at the surface, AFGL mid-latitude and summer atmosphere model, $\theta_o=30^\circ$, $\theta_s=0^\circ$, $\phi=0^\circ$, snow surface, the H–G phase function and $g=0.9$).

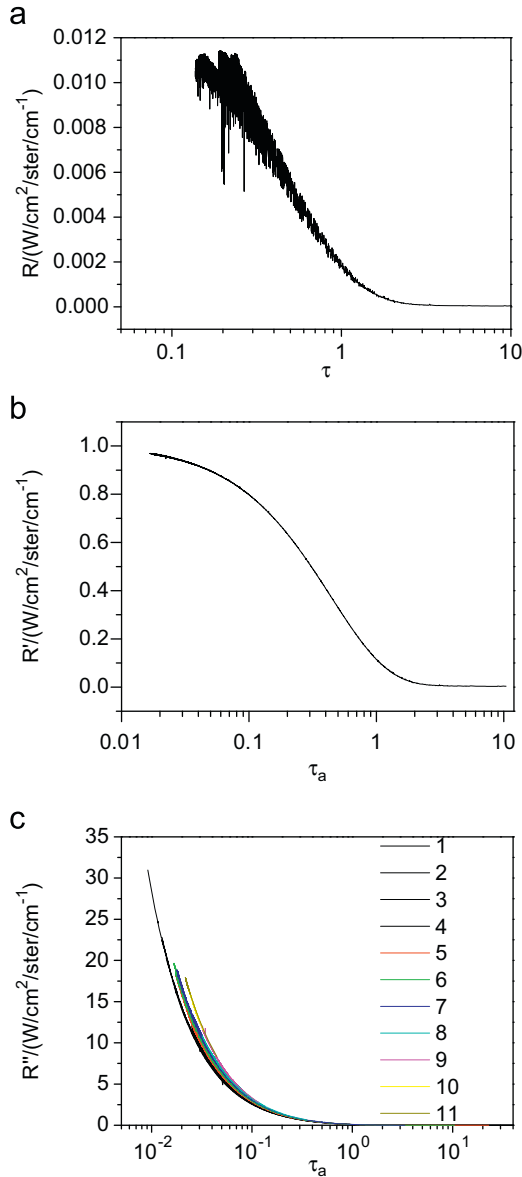


Fig. 2. The relationship between radiative parameters vs. optical parameters: (a) radiances R vary greatly with total optical thicknesses τ ; (b) radiances divided by surface albedos R' vary smoothly with absorption optical thicknesses τ_a and (c) radiances divided by absorption optical thicknesses and by scattering optical thicknesses R'' vary smoothly with τ_a in each subspectrum, the spectral interval of subspectrums from 1 to 3 is 1000 cm^{-1} , and interval of the others is 2500 cm^{-1} , the other parameters are the same as Fig. 1.

5000 cm^{-1} will be treated separately. We refer to wavenumbers $2001\text{--}5000 \text{ cm}^{-1}$ as band 1 and wavenumbers $5001\text{--}25,000 \text{ cm}^{-1}$ as band 2. After analysis of many cases, we found a 1000 cm^{-1} interval in band 1 and a 2500 cm^{-1} interval in band 2 to provide sufficient accuracy without a loss of computational efficiency. With this approach, only 11 sub-regions (the digital 1–11 shown in Fig. 2(c)) are necessary in the region from 2001 cm^{-1} to $25,000 \text{ cm}^{-1}$. The band interval of the first

3 sub-regions is 1000 cm^{-1} , and the band interval of the other 8 sub-regions is 2500 cm^{-1} .

To summarize our approach, we propose a fast method to compute scattered radiance of a clear atmosphere based on the τ_s , τ_a surface albedo within the 11 sub-regions of the spectral range from 2001 to $25,000 \text{ cm}^{-1}$. For each sub-region, the pre-computed τ_a obtained from the CSRTM are sorted in ascending order. The functional relationship between R' or R'' and τ_a is used to compute the multiple scattering radiance component using DISORT for specific wavenumbers within each sub-region. For each selected wavenumber, the calculated scattered radiance by DISORT $R(v_0)$ is treated as follows:

$$R'(v_0) = \frac{R(v_0)}{r_s(v_0)},$$

for the case of upward radiances from the surface, (5)

$$R''(v_0) = \frac{R(v_0)}{\tau_s(v_0)\tau_a(v_0)},$$

for the other cases. (6)

where r_s is the surface albedo and v_0 is the selected wavenumber. With the use of a spline fitting method, $R'(v)$ or $R''(v)$, for any wavenumber v , is interpolated according to the pre-computed τ_a as shown in Fig. 3. The total number of $R'(v_0)$ or $R''(v_0)$ chosen to perform the exact DISORT calculations will affect the accuracy and efficiency of EMASR. We found the adoption of 7 nodes of $R'(v_0)$ or $R''(v_0)$ to provide sufficient accuracy while still maintaining computational efficiency. Fig. 4 shows the comparisons between the results from DISORT and from the proposed fast model by using 8 nodes, 7 nodes, and 6 nodes of $R'(v_0)$ or $R''(v_0)$. The fitted values obtained using 8 nodes or 7 nodes are close to the DISORT results, while by using 6 nodes relatively large errors appear. Therefore, we have chosen to use 7 nodes in our fitting method. By using the proposed fast fitting method, the $R'(v)$ or $R''(v)$ at other wavenumbers can be computed efficiently and with good accuracy. Given the solar light incidence I_s at the TOA, the final radiance at any wavenumber v can be obtained as follows:

$$R(v) = R'(v)r_s(v)I_s(v)/\pi,$$

for the case of upward radiances from the surface (7)

$$R(v) = R''(v)\tau_s(v)\tau_a(v)I_s(v)/\pi,$$

for the other cases. (8)

3. Accuracy and timing cost test

This section provides the estimate of the accuracy and efficiency of the EMASR method for calculating the scattered radiance in a clear atmosphere along an arbitrary path. The accuracy will be assessed by investigating the differences between the EMASR and DISORT methods at each spectral point. At the same time, we will compare the computational requirements of each of the two methods.

For both methods, the CSRTM is used to compute the optical thickness due to absorption of molecules and aerosols from 2001 cm^{-1} to $25,000 \text{ cm}^{-1}$ with a 1 cm^{-1} interval. In DISORT, the scattering and absorption of each layer $\tau_{a,l}$, $\tau_{s,l}$ at all spectral points along the path are

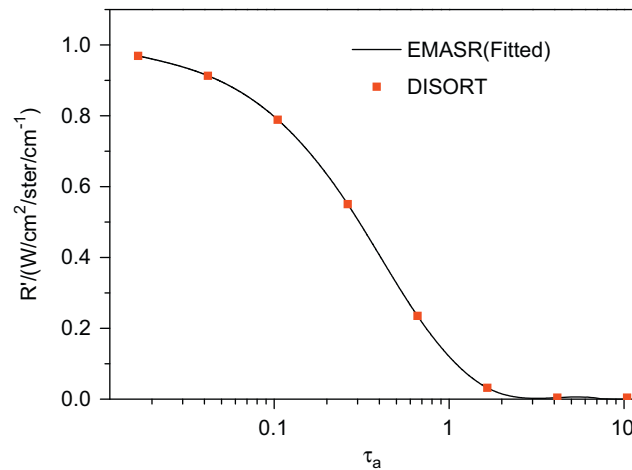


Fig. 3. Comparison of fitted R' with the original data calculated directly by using DISORT (red dot: the original data calculated directly by using DISORT; black line: the fitted data, case of upward radiance at the top of atmosphere, in the spectral region is from 10,000 to 12,500 cm^{-1}). (For interpretation of the references to color in this figure legend, the reader is referred to the web version of this article.)

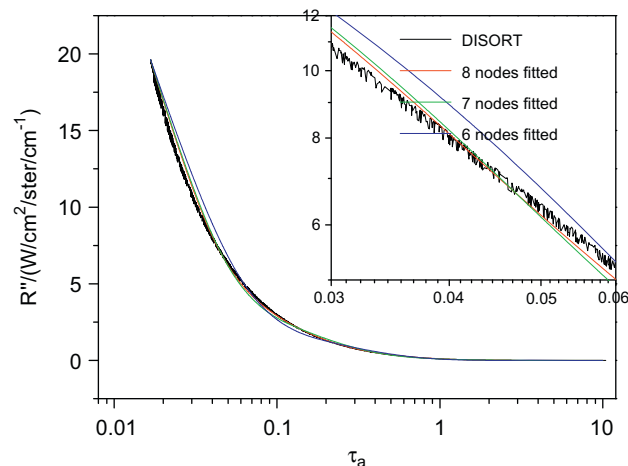


Fig. 4. Comparison of DISORT with different kind of fitting methods (black line: the original data calculated by using DISORT; red, green and blue lines are the fitted data using 8, 7 and 6 nodes fitting method, respectively, case of downward radiance at surface, 10,000–12,500 cm^{-1}). (For interpretation of the references to color in this figure legend, the reader is referred to the web version of this article.)

Table 1
Parameters of four test cases.

| Cases | Radiance orientations | Transfer paths |
|-------|-----------------------|----------------------------------|
| A | Upward | Surface to the top of atmosphere |
| B | Downward | TOA to the surface |
| C | Upward | 5 km height to TOA |
| D | Downward | 10 km height to the surface |

computed, while in the EMASR, the scattering and absorption of each layer are computed at only selected spectral points. For both DISORT and EMASR calculations, the phase function is decomposed into Legendre polynomials using the δ -fit approach, and performed assuming 16 streams.

Four cases are investigated (Table 1): two cases at the TOA (case A from the surface and C from 5 km) and two

cases at the surface (case B from the TOA and D from 10 km). Case A includes reflected radiance by the surface, while cases B, C and D compute the scattering from the atmosphere without reflection from the surface. The treatments for the cases with and without surface reflection are different (see Eqs. (5) and (6)). Cases C and D illustrate the EMASR can be used to compute scattering for any arbitrary path in the atmosphere. A middle-latitude summer atmospheric model is assumed, with a rural aerosol loading in the atmospheric column for which the H–G phase function with an asymmetry factor of $g=0.9$ is assumed to represent the scattering phase function of the rural aerosols. Assumptions for the other parameters are: the solar zenith angle is $\theta_s=0^\circ$, the viewing zenith angle is $\theta_o=30^\circ$, the surface visibility is 23 km, the surface albedo is a function of wavenumber, and the surface temperature is 290 K. The results are shown in Fig. 5. From the figure, it is evident the EMASR is

quite accurate, as the relative differences (RD) between the EMASR and DISORT are 0.55%, 1.83%, 1.69%, and 1.69%, for cases a, b, c, and d, respectively. The RD value is

defined as

$$RD = \frac{RMS(\Delta R)}{R_D} \times 100\% \quad (9)$$

$$RMS(X) = \sqrt{\frac{\sum_i^N (X_i)^2}{N}} \quad (10)$$

where N is the number of spectral points in the spectrum, R_D is the mean radiance calculated by using DISORT, ΔR is the difference between EMASR and DISORT, RMS is the root mean square, and X_i is the value at the i th spectral point.

The computational burden is separated into three parts: (I) computing the optical thickness by CSRTM, (II) expanding the scattering phase function, and (III) calling the DISORT subroutine. The computational cost of obtaining the atmospheric optical thickness from the CSRTM is inconsequential compared to that required for steps II and III. Computations for parts II and III are performed at every wavenumber in DISORT, while they are necessary for only 7 wavenumbers within each sub-region in EMASR. The computational efficiency depends on how many times DISORT is called relative to EMASR. For a sub-region of 1000 cm^{-1} spectral width, parts II and III will be performed 1000 times in the DISORT method but only 7 times in the EMASR, making the EMASR approximately 140 times faster than the DISORT method. Similarly, the EMASR will be 350 times faster than directly calling the DISORT model in wavebands of 2500 cm^{-1} intervals. For case (B) in Fig. 5 ($2001\text{--}25,000 \text{ cm}^{-1}$), the computation by EMASR takes 3 mins on a 3.2 GB Intel Pentium 4 personal computer, while a similar calculation by DISORT takes more than 12 h. On the same personal computer, the speed of the EMASR is about 240 times faster for atmospheric scattering radiance computations in the spectral region from 2000 cm^{-1} to $25,000 \text{ cm}^{-1}$ (23,000 spectral points).

4. Applications to FTIR downwelling radiance simulation

The Fourier transform infrared (FTIR) interferometer (MR170 series) measures downwelling spectral radiance with a resolution of $\sim 1 \text{ cm}^{-1}$ in the range of infrared wavelengths from 2 to $15 \mu\text{m}$. The data may be used to evaluate EMASR accuracy by comparing the simulated and measured spectra.

The FTIR interferometer uses two infrared detectors to achieve a wide spectral range, the MCT detector measures the spectrum from about 700 to 1800 cm^{-1} , and the InSb detector from about 2000 to 5000 cm^{-1} . The two detectors are cooled to the boiling point of liquid nitrogen to reduce the noise equivalent differential temperature (NEdT). A mirror with a middle field of view is assembled

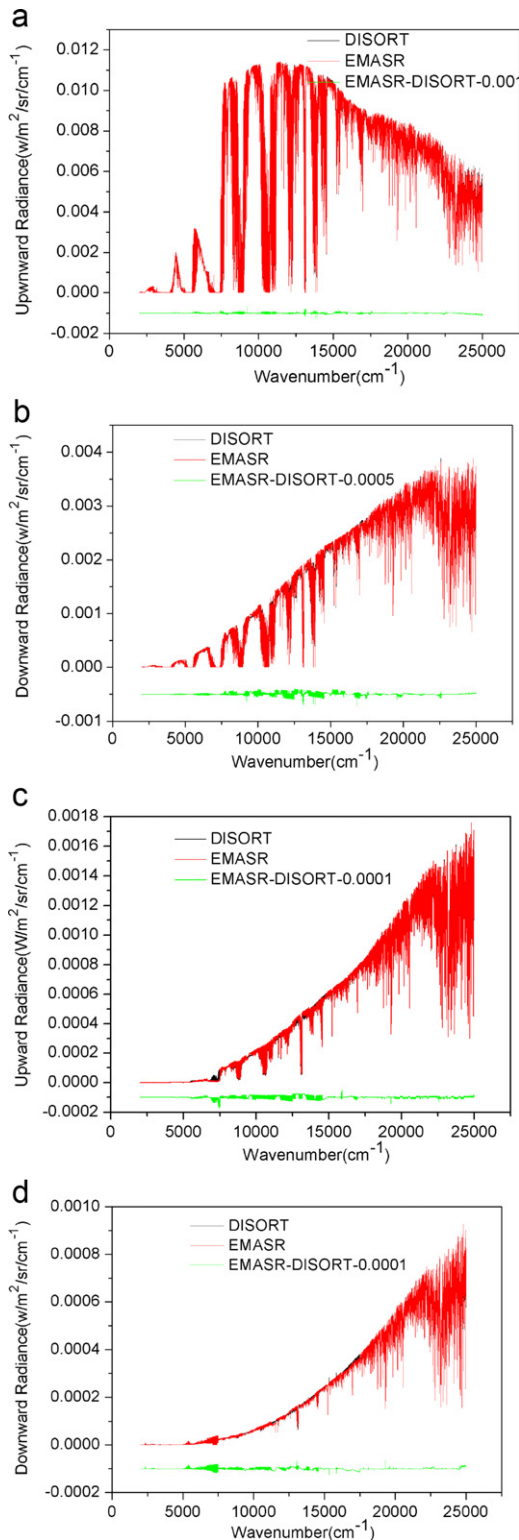


Fig. 5. Comparisons of EMASR with DISORT on clear condition (black line: calculated by DISORT; red line: calculated by EMASR; green line: the difference of between EMASR and DISORT: (a) upwelling at the top of atmosphere from surface, (b) downwelling at surface from the top of atmosphere, (c) upwelling at the top of atmosphere from 5 km height, (d) downwelling at surface from 10 km height.). (For interpretation of the references to color in this figure legend, the reader is referred to the web version of this article.)

on the FTIR system. As the FTIR system is fixed outside, a mirror with high reflectivity (> 0.97) is sealed on the front. By turning the mirror, the FTIR interferometer can be used to collect atmospheric signals at different zenith and azimuth angles. The collected data are calibrated to spectral radiances by using two blackbody targets (at 30 and 140 °C), which provide two reference spectra to determine the gains and offsets of the detectors and associated electronics.

Then EMASR is applied to simulate the FTIR interferometer observed clear sky radiances at 12:40 Beijing time on 4 April 2010 in Hefei, China. The observing zenith angle is 45°, the observing azimuth angle is 140°, the solar zenith angle is 25.4°, the solar azimuth angle is 164°, the surface temperature is 288.7 K, and the surface visibility is 8 km. The profiles of real time temperature, pressure and relative humidity are from a meteorologic radio-sounding, and the ozone profile is from the AFGL mid-latitude summer profile with a scaling factor. The scattering phase function is assumed to be the H-G function with $g=0.9$.

Two wave band comparisons are shown: the 700–1400 cm^{-1} band, in which the thermal radiance mainly occurs; and the 3000–5000 cm^{-1} band, in which the scattering radiance from the sun is predominant. Fig. 6(a) shows the comparison between simulated upwelling

brightness temperatures (BTs) with FTIR interferometer measured BTs in the region from 700 to 1400 cm^{-1} . Fig. 6(b) shows the comparison between simulated upwelling radiances with FTIR interferometer measured radiances in the region from 3000 to 5000 cm^{-1} . In the figures, the measured and simulated data are averaged to a 2 cm^{-1} spectral resolution. The figures indicate the simulated data coincides well with the measured data in both the regions. The RMS difference of BTs between measured and simulated BTs is 3.0 k in the first region, while the error in the second region is only 3.1×10^{-9} ($\text{W}/\text{cm}^2/\text{ster}/\text{cm}^{-1}$). The difference is primarily a result from the mismatch of spectral resolution and wavenumber between EMSAR and FTIR interferometer.

5. Applications to AIRS upwelling radiance simulations

The Atmospheric Infrared Sounder (AIRS) [13] was designed to provide high accuracy profiles of atmospheric temperature, moisture, and other gases. Because the observed AIRS fields of view may encompass molecular absorption, aerosols, thin ice clouds, and/or thick water clouds, the simulation of AIRS radiances must be able to account for these factors. To demonstrate its performance, the EMASR is

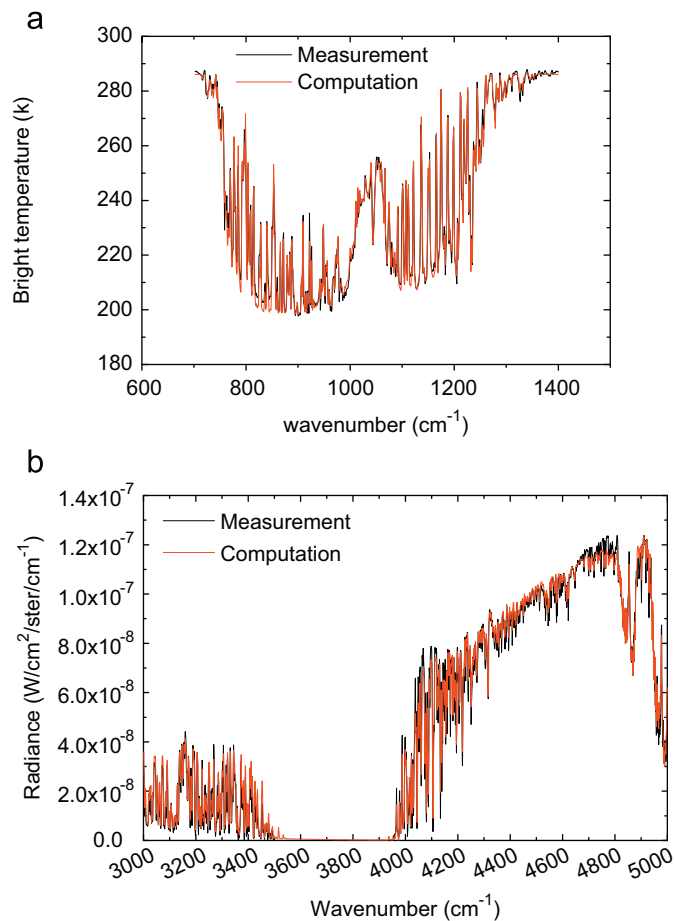


Fig. 6. Comparison between simulated upwelling BTs (a) and radiances (b) with FTIR interferometer observed data.

applied to AIRS spectral radiance computations under both clear and cloudy conditions (water and ice clouds).

Single-layered clouds are assumed to reside in a plane-parallel, homogeneous and isothermal layer in a given field of view (FOV). Bulk cloud single-scattering properties are required to specify the radiative effects in a radiative

cloud scattered radiance computations are expensive and a fast method is employed.

For a cloud residing in the n_{cld} layer, the total scattering from the cloud particles, including the contribution of aerosols and molecules, the single-scattering albedo ω , and phase function P may be described by

$$\omega(n_{cld}) = \frac{\tau_{ms}(n_{cld}) + \tau_{as}(n_{cld}) + \tau_{cs}(n_{cld})}{\tau_{ms}(n_{cld}) + \tau_{ma}(n_{cld}) + \tau_{mc}(n_{cld}) + \tau_{as}(n_{cld}) + \tau_{aa}(n_{cld}) + \tau_{cs}(n_{cld}) + \tau_{ca}(n_{cld})} \quad (12)$$

transfer model. A database was prepared containing parameterized coefficients of the single-scattering properties of water clouds and 5 kinds of ice clouds (assumed ice particle habits as aggregates of columns, hollow and solid columns, hexagonal plates, and 3D solid bullet rosettes) from 1 to 25,000 cm^{-1} with a 1 cm^{-1} spectral resolution. The single-scattering parameters for water clouds are computed with a Lorentz–Mie code, while the single-scattering properties of ice clouds are from Yang et al. [14,15]. A least square fitting method is used to parameterize the single-scattering properties as a function of effective particle size D_e . The D_e or the effective radius ($D_e/2$) of either water or ice clouds and the wavelength are the only data necessary to obtain the single-scattering properties of extinction efficiency $\langle Q_e \rangle$, absorption efficiency $\langle Q_a \rangle$, and asymmetry factor $\langle g \rangle$. For a cloud in the n_{cld} layer with a reference visible optical thickness τ_{vis} (at a visible wavelength of 0.55 μm , i.e., a wavenumber of 18,181 cm^{-1}), the optical thickness at wavelength λ is

$$\tau_c = \frac{\langle Q_{e,\lambda} \rangle}{\langle Q_{e,vis} \rangle} \tau_{vis} = \tau_{cs} + \tau_{ca} = \frac{\langle Q_{s,\lambda} \rangle + \langle Q_{a,\lambda} \rangle}{\langle Q_{e,vis} \rangle} \tau_{vis}, \quad (11)$$

where τ_{cs} and τ_{ca} are the scattering and absorption optical thicknesses of clouds.

For both clear and cloudy atmospheres, the thermal radiance and scattered radiance are computed. The upward or downward thermal radiance in a cloudy atmosphere is composed of 4 parts as described by Wei et al. [6]. While the thermal radiances for both clear-sky and cloudy conditions can be computed efficiently, the

and

$$p(n_{cld}) = \frac{\tau_{ms}(n_{cld})p_m(n_{cld}) + \tau_{as}(n_{cld})p_a(n_{cld}) + \tau_{cs}(n_{cld})p_c(n_{cld})}{\tau_{ms}(n_{cld}) + \tau_{as}(n_{cld}) + \tau_{cs}(n_{cld})} \quad (13)$$

The entire waveband is divided into 13 sub-regions; the spectral region from 2001 to 25,000 cm^{-1} is divided into 11 sub-regions, and the spectral region from 1 to 2000 cm^{-1} is divided into two sub-regions. The EMASR is applied to the AIRS data over a more limited wavenumber range from 650 to 2700 cm^{-1} . For simulating the AIRS radiances at the TOA, the thermal radiance is included in the simulation, and the results are provided in terms of the equivalent brightness temperature (BT).

Fig. 7 shows the TOA brightness temperatures at the TOA for AIRS simulations from both EMASR and DISORT; the differences between the two are shown in the lower panel. Three cases are studied: one for clear-sky, one for ice clouds with $\tau_{vis}=1.0$ (optically thin) at a height of 11 km, and one for water clouds with $\tau_{vis}=10.0$ (optically thick) at a height of 2 km. The single-scattering properties for ice cloud are assumed to be represented solely by aggregates. The effective particle size for the ice cloud is assumed to be 50 and 10 μm for water clouds. For both the ice/water layer, the scattering phase function is given by the H–G phase function with $g=0.9$. The atmospheric profiles used in CSRTM are provided from the European Center for Medium-Range weather Forecasts (ECMWF) model data. The RMS of the difference of the TOA brightness temperature between EMASR and DISORT provides an index for the error of EMASR in the IR waveband, and is given by Eq. (10). The

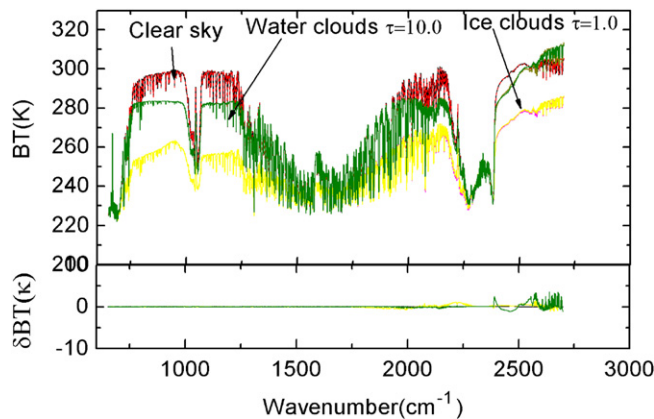


Fig. 7. Comparisons the spectral brightness temperatures for AIRS infrared wavelength bands between EMASR with DISORT for clear-sky, cirrus sky and water cloud-sky. Deviations shown in bottom panel.

Table 2
Specifications for three cases in AIRS data simulations.

| | Condition | θ_s ($^\circ$) | θ_o ($^\circ$) | τ_{vis} | r_e (μm) | H_c (km) | T_s (K) |
|--------|--------------------|-------------------------|-------------------------|--------------|-------------------------|------------|-----------|
| Case 1 | Clear | 33.1 | 6.8 | 0.0 | – | – | 310.3 |
| Case 2 | Thin ice clouds | 33.1 | 24.1 | 0.85 | 100.0 | 9.0 | 310.2 |
| Case 3 | Thick water clouds | 40.3 | 51.1 | 5.8 | 15.0 | 6.55 | 302.5 |

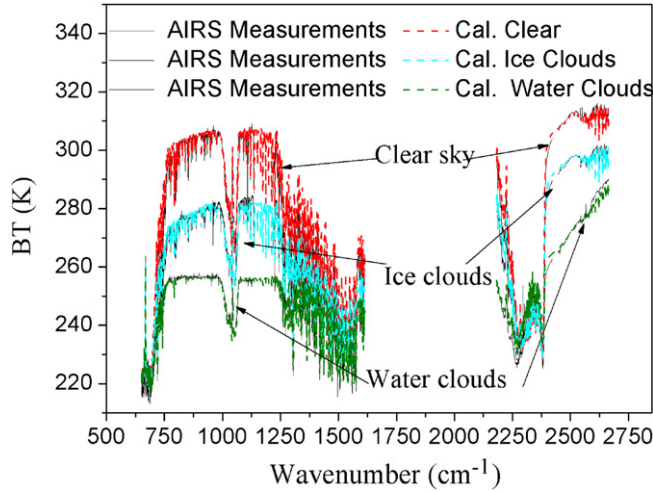


Fig. 8. Comparison between simulated upwelling BTs with AIRS observed BTs for clear-sky case, ice cloud-sky case, and water cloud-sky case.

NEDTs in the first band of AIRS, from 650 to 2000 cm^{-1} , are relatively constant at a level of 0.2 K. The NEDTs increase in the second band between 2001 and 2665 cm^{-1} where most of the solar scattering takes place. The RMS for clear atmosphere, ice clouds and water clouds are $3.2\text{E}-5$, 0.12 and 0.03 K, respectively, in the first band, but increase to 0.05, 0.35 and 0.77 K, respectively, in the second band. However, these values are approximately the same as the AIRS sensor measured NEDTs.

The EMASR is applied to select fields of view in an AIRS granule measured for a case study at 1917 UTC on 6 September 2002. The fields of view are chosen from clear sky, cirrus clouds, and optically thick water clouds with the identification of the clouds from collocated MODIS data. The solar zenith angle (θ_s), satellite observing zenith angle (θ_o), visible optical thickness (τ_{vis}), effective radius (r_e), cloud height (H_c), and surface temperature (T_s) of each case are shown in Table 2. The results between simulated upward BTs and AIRS observed data are shown in Fig. 8. From Fig. 8, it is shown the simulated results from EMASR coincide well with the AIRS high spectral observations, both for clear-sky and cloudy conditions. The differences of BTs between EMASR simulation and AIRS observations are not shown, because the spectral resolution of AIRS may vary, by $v/\Delta v = 1200$, where v is the wavenumber and Δv is the width of a band, while the spectral resolution of EMASR is a constant of 1 cm^{-1} . The results illustrate the fast model EMASR can be used to quickly simulate the moderate spectral resolution (including low spectral resolution) observations, such as the

AIRS observed data, for both clear and cloudy sky conditions (ice clouds and thick water clouds).

6. Summary and discussion

This study discusses the development of a fast method for atmospheric scattering radiance calculation referred to as EMASR. The spectral range is from 1 to 25,000 cm^{-1} with a 1 cm^{-1} resolution, and multiple scattering is considered over the entire waveband. The algorithm can be used for computing scattering radiance from atmospheric molecular constituents and aerosols, and for ice and water clouds. The EMASR makes use of fitting DISORT calculated values at uniformly spaced nodes of logarithmic absorbing optical thicknesses in a sub-spectrum. The gain in computational speed is 140 to 350 orders of magnitude compared to the use of DISORT at each wavenumber.

Accuracy tests show the relative standard difference between EMASR and DISORT is less than 2% in a clear-sky atmosphere. RMS values of EMASR brightness temperatures at TOA for AIRS channels over clear-sky and ice/water clouds are within the NEDTs of AIRS sensors. The RMS values for cloudy sky are larger than for clear-sky, because the function of scattered radiances in a cloudy atmosphere does not vary as smoothly with τ_a, τ_s as under clear-sky conditions. Further refinement may reduce the error and will be investigated in future work.

Comparisons of the fast EMASR method with FTIR interferometer measured downwelling radiances and with

AIRS measured upwelling BTs were performed, and the simulated data, in general, agreed with the measurements for both clear-sky and cloudy cases. The fast method may be useful for cloud remote sensing in the visible to infrared spectrum with moderate spectral resolution.

Acknowledgment

Heli Wei acknowledges supports by the National Natural Science Foundation of China (NSFC) under the grant 61077081, and the Knowledge Innovation Foundation of the Chinese Academy of Sciences.

References

- [1] Stamnes K, Tsay SC, Wiscombe WJ, Jayaweera K. Numerically stable algorithm for discrete-ordinate-method radiative transfer in multiple scattering and emitting layered media. *Appl Opt* 1988;27:2502–9.
- [2] Meador WE, Weaver WR. Two-stream approximation to radiative transfer in planetary atmospheres: a unified description of existing methods and new improvement. *J Atmos Sci* 1980;37:1279–90.
- [3] Liou KN. Analytic two-stream and four-stream solutions for radiative transfer. *J Atmos Sci* 1974;31:1279–90.
- [4] King MD, Harshvardhan. Comparative accuracy of selected multiple scattering approximations. *J Atmos Sci* 1986;43:784–801.
- [5] Cuzzi JN, Ackerman TP, Helmle LC. The delta-four-stream approximation for radiative flux transfer. *J Atmos Sci* 1982;39:917–25.
- [6] Wei HL, Yang P, Li J, Baum BA, Huang HL, Platnick S, et al. Retrieval of semitransparent ice cloud optical thickness from atmospheric infrared sounder (AIRS) measurements. *IEEE Trans Geosci Remote Sensing* 2004;42:2254–67.
- [7] Niu JG, Yang P, Huang HL, James E, et al. A fast infrared radiative transfer model for overlapping clouds. *J Quant Spectrosc Radiat Transfer* 2007;103:447–59.
- [8] Zhang Z, Yang P, Kattawar GW, Huang HL, Greenwald T, Li J, Baum BA, Zhou DK, Hu YX. A fast infrared radiative transfer model based on the adding-doubling method for hyperspectral remote sensing applications. *J Quant Spectrosc Radiat Trans* 2007;105:243–63.
- [9] Moncet JL, Clough SA. Accelerated monochromatic radiative transfer for scattering atmospheres: application of a new model to spectral radiance observations. *J Geophys Res* 1997;102:21853–66.
- [10] Clough SA, Iacono MJ. Line-by-line calculation of atmospheric fluxes and cooling rates. 2. Application to carbon dioxide, ozone, methane, nitrous oxide and the halocarbons. *J Geophys Res* 1995;100:16519–35.
- [11] Wei HL, Chen XH, Rao RZ, et al. A moderate-spectral-resolution transmittance model based on fitting the line-by-line calculation. *Opt Express* 2007;15:8360–70.
- [12] Hu YX, Wielicki B, Lin B, Gibson G, Tsay SC, Stamnes K, Wong T. A fast and accurate treatment of particle scattering phase functions with weighted singular-value decomposition least-squares fitting. *J Quant Spectrosc Radiat Trans* 2000;68:681–90.
- [13] Aumann HH, Chahine MT, Gautier C, Goldberg MD, Kalnay E, Mcmillin LM, Revercomb MH, Rosenkranz PW, Smith WL, Staelin SH, Strow LL, Susskind. AIRS/SMSU/HSB on the Aqua mission: design, science objectives, data product, and processing systems. *IEEE Trans Geosci Remote Sensing* 2003;41:253–64.
- [14] Yang P, Liou KN, Wyser K, Mitchell D. Parameterization of scattering and absorption properties of individual ice crystals. *J Geophys Res* 2000;105:4699–718.
- [15] Yang P, Wei HL, Huang HL, Baum BA, Hu YX, Kattawar GW, Mishchenko MI, Fu Q. Scattering and absorption property database for nonspherical ice particles in the near- through far-infrared spectral region. *Appl Opt* 2005;44:5512–23.